frontiers in Energy Research

ORIGINAL RESEARCH
published: 17 November 2021
doi: 10.3389/fenrg.2021.765519

Effect of Different CO_2 Treatments on the Metal Leaching in Steel Slag Binders

Yaojun Liu[1], Jingrui Fang[1], Songhui Liu[2], Xiaopeng An[1], Yanwen Kang[1] and Lan Wang[1]*

[1]State Key Laboratory of Green Building Materials, China Building Materials Academy, Beijing, China, [2]School of Materials Science and Engineering, Henan Polytechnic University, Jiaozuo, China

Carbonation is an effective method to promote the quality of the steel slag binder. In this article, two carbonation approaches, namely hot-stage carbonation and accelerated carbonation, were employed to leach the metals, and the influence mechanism on the metal sequential leachability of the binders composed of 80 wt% of EAF slag incorporating 20 wt% of Portland cement (PC) was revealed. The carbonate products, microstructures, and chemical states were investigated, and the results indicated that chromium, vanadium, and titanium gradually transformed into inactive phases after two carbonation approaches, while zinc appeared the opposite trend. The sequential leachability of chromium declined with the increase of the carbonation efficiency, in which the exchangeable chromium decreased from 1.99 mg/kg in the A2A binder to below the detection limit in the A2C binder and C2C binder. Hot-stage carbonation treatment facilitated particle agglomeration, minerals remodeling, and calcite formation. The carbonation curing of the steel slag paste resulted in the formation of amorphous $CaCO_3$, calcite crystalline and Si-bearing hydrates that covered the pores of the matrix, and silicate structure with a higher disorder. The hot-stage carbonation and accelerated carbonation curing methods were adopted to jointly prevent the leaching of harmful metals and facilitate promising high-volume steel slag-based binders with structural densification and CO_2 storage.

Keywords: accelerated carbonation curing, CO_2 storage, sequential leachability, steel slag, hot-stage carbonation

OPEN ACCESS

Edited by:
Shuiping Yan,
Huazhong Agricultural University, China

Reviewed by:
Hai Yu,
Commonwealth Scientific and Industrial Research Organisation (CSIRO), Australia
Rafael Mattos Dos Santos,
University of Guelph, Canada

****Correspondence:***
Yaojun Liu
liuyaojunpaper@yeah.net

Specialty section:
This article was submitted to Carbon Capture, Utilization and Storage, a section of the journal Frontiers in Energy Research

Received: *27 August 2021*
Accepted: *06 October 2021*
Published: *17 November 2021*

Citation:
Liu Y, Fang J, Liu S, An X, Kang Y and Wang L (2021) Effect of Different CO_2 Treatments on the Metal Leaching in Steel Slag Binders. Front. Energy Res. 9:765519. doi: 10.3389/fenrg.2021.765519

INTRODUCTION

Steel slags, the inevitable industrial waste in the process of steel manufacturing, account for 15–35% of crude steel (Eloneva et al., 2010). In China, the annual output of steel slags exceeds 100 million tons (Guo et al., 2018), but the utilization ratio is below 30% (Pan et al., 2017). Steel slags are mainly recycled for the fields of cement and concrete (Carvalho et al., 2017), road building (Pasetto and Baldo, 2016), bituminous mixture (Skaf et al., 2017), soil amelioration (Poh et al., 2006), and phosphate fertilizer (Yi et al., 2012). However, the utilization of the steel slag was restricted by the slow hydration and the undesired deleterious expansion due to the mineralogical changes, such as the hydration of the free CaO and MgO and the transformation of α-C_2S (Wang et al., 2010; Mo et al., 2017).

The carbonation of steel slags was proved as an effective method to solve these issues, which was due to the slower hydration reaction of steel slag than that of the carbonization in the humid environment and the improvement of mineralogical stability by the carbonization of the alkaline oxides (Ukwattage et al., 2017). Meanwhile, the carbonation of steel slags contributed to the storage of CO_2. Several researchers investigated the potential application of steel slags for carbon

FIGURE 1 | Photos of original EAF steel slag **(A)** and carbonated EAF slag **(B)**.

sequestration to produce qualified building materials (Polettini and Pomi, 2004; Baciocchi et al., 2015; Kim et al., 2016; Pan et al., 2017). Moreover, hot-stage CO_2 sequestration not only provided recovery potential but also reused the waste heat from the exhaust gas to accelerate reactions, which could be a finishing step in the industrial plants (Pan et al., 2016).

According to previous studies, carbonation changed the performance of the steel slag, and much more attention should be paid to the leaching of hazardous elements (e.g., Cr, V, and Mo) (Belhadj et al., 2012). The steel slags from the stainless-steel production contain a lower FeO content but a higher Cr content (Shi, 2004). There were only limited studies about the mechanism between the carbonation and the leaching of hazardous elements. Kim et al. (Kim et al., 2016) stated that the leachability of Cr decreased from 0.8 mg/kg to 0.4 mg/kg based on the one-stage leaching tests of the carbonated stainless-steel slag. Ya-jun Wang et al. (Wang et al., 2020) performed the static thin-film accelerated carbonation and sequential leaching tests on the AOD steel slag and stated that the leachability of Cr increased with the growth of the carbonation ratio, reaching the highest leaching value of 7.9 mg/kg at 52% of the carbonation ratio. However, there was a dearth of further study on the influence mechanisms of the CO_2 accelerated treatment processes on the leachability of hazardous elements, which is important to prevent the potential of toxicity and promote the high blended proportion use of steel slag in the construction materials.

Herein, the influences of two different CO_2 treatment processes on the metal leachability and valence states were investigated based on the pastes of 80% steel slags. Two carbonation approaches were adopted for comparison, including hot-stage carbonation (applied during pretreatment of steel slag with simulated gas) and post carbonation (applied during post-curing). The Tessier sequential extraction was carried out to determine the different chemical profiles of the metal elements in these specimens. The mineralogical, CO_2 uptake, and microstructural properties were specifically investigated and compared to analyze the influence of carbonation on the leachability of metal elements in the end products.

MATERIALS AND METHODS

Materials

The original electric arc furnace steel slags (SS for short) were obtained from one steel plant in Shandong Province, China. The EAFs were ground and sieved to less than 200 μm, which is shown in **Figure 1A**. According to the results of Ca-Looping (CaL) process (Miranda-Pizarro, et al., 2016; Tian, et al., 2014) and fast absorption of CO_2 by steel slag (Dong, 2008; Stolaroff, et al., 2005), the hot-stage carbonation of SS was proposed to carbonate the free calcium oxide in SS. The carbonated EAF slags (CSS for short) were obtained by the raw EAF slags heated at 650°C in a 99.9 vol% of CO_2 stream atmosphere under the atmospheric pressure, which is shown in **Figure 1B**. The reference cement (RC for short)was the 42.5-grade cement provided by Fushun Cement Co. Ltd. in Liaoning Province. **Table 1** lists the chemical composition of SS, CSS, and RC determined by XRF. XRD and TG-DSC analysis of original EAF steel slag and carbonated EAF slag are shown in **Figure 2**. The results indicated that the most relevant mineralogical phases, including dicalcium silicate (Ca_2SiO_4), the RO phase, srebrodolskite ($Ca_2Fe_2O_5$), and Brownmillerite ($Ca_2(Al,Fe)_2O_5$) stayed almost the same after hot-stage carbonation process, while the diffraction peak of hatrurite (Ca_3SiO_5) decreased during hot-stage carbonation, confirming the results of other studies on EAF slag (Wu et al., 2015). The carbonation efficiency (hereinafter referred to as EOC) was widely used to estimate the carbonation performance of various building materials or solid wastes by TG-DSC analysis (Chang and Fang, 2015; Liu and Wang, 2018). Mass change of calcite decomposition of the carbonated EAF slag samples was 1.13%, and the EOCs of the EAF slag samples were 3.45% after hot-stage carbonation process.

Production and Carbonation of Granulated EAF Slag Binders

Three different carbonation procedures were designed to investigate the effects of CO_2 on the performances of the produced EAF slag binders, as listed in **Table 2**. As indicated

TABLE 1 | Chemical composition of steel slag and reference cement.

Sample	f- CaO	f- MgO	Fe_2O_3	CaO	SiO_2	MgO	Al_2O_3	MnO	P_2O_5	TiO_2	Cr_2O_3	SO_3	V_2O_5	Na_2O	ZnO
Raw EAF slag(R)	1.72	0.29	34.12	30.99	16.3	7.76	3.78	3.3	1.49	0.7	0.44	0.277	0.273	0.258	0.025
Carbonated EAF slag(C)	0.36	0.077	34.12	30.74	16.58	7.63	3.92	3.3	1.5	0.696	0.437	0.279	0.273	0.219	0.029
References cement	0.88	—	3.62	63.56	20.12	2.07	5.12	—	—	—	—	2.38	—	0.53	—

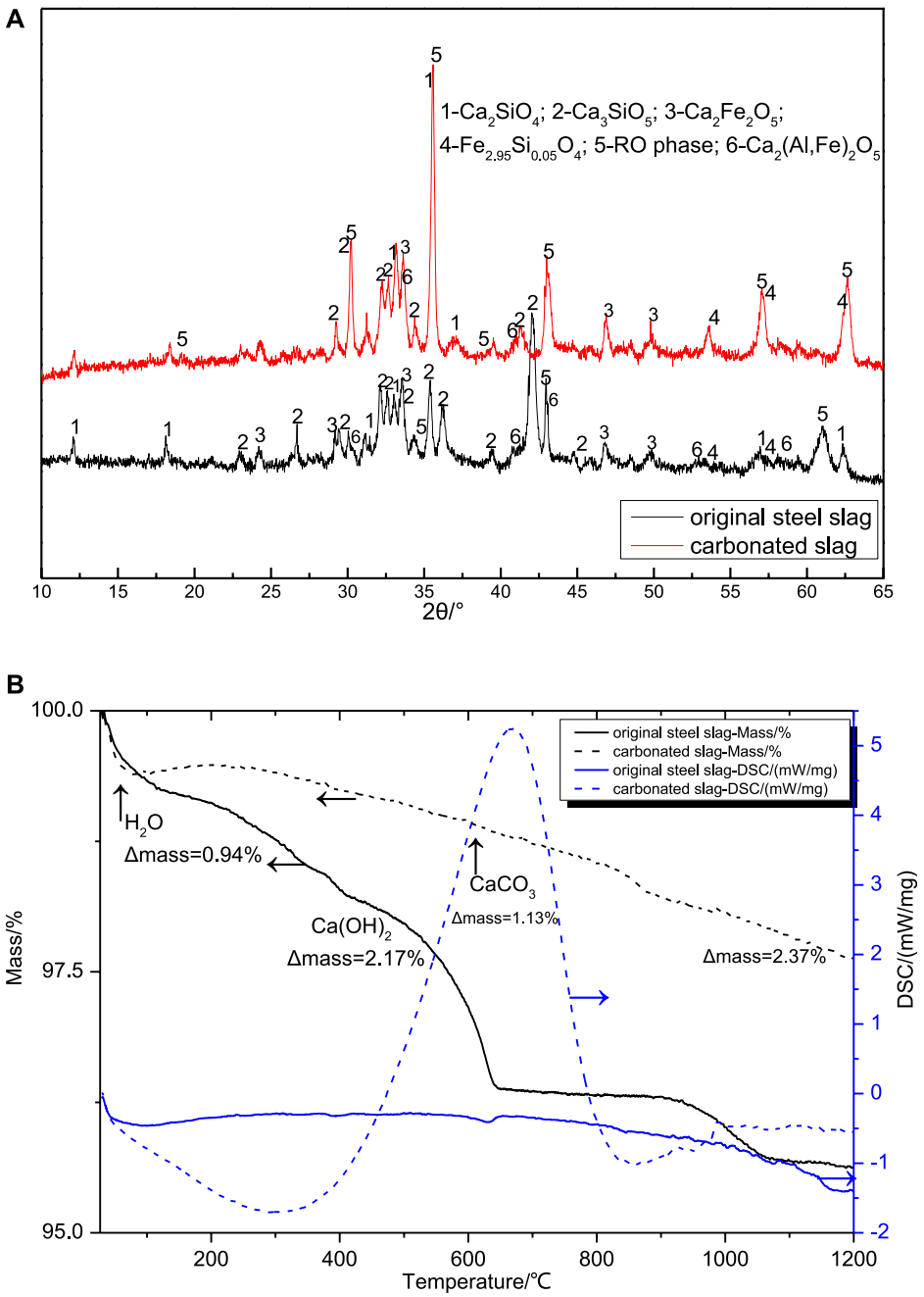

FIGURE 2 | XRD **(A)** and TG-DSC **(B)** analysis of original EAF steel slag and carbonated EAF slag. (1–6 of **Figure 2A** denote larnite, calcium silicate, srebrodolskite, iron silicon oxide, RO phase, and brownmillerite, respectively.).

TABLE 2 | Carbonation procedures.

Notation	Carbonation procedure	Proportion/%	Note
C2C	hot-stage CO_2 pretreatment and accelerated carbonation curing	80% Carbonated EAF slag + 20% RC	for the binders that were made of carbonated EAF slag and demoulded into the post-curing treatment
A2C	accelerated carbonation curing	80% raw EAF slag + 20% RC	for the binders that were made of raw EAF slags and demoulded into the post-curing treatment
A2A	no carbonation	80% raw EAF slag + 20% RC	for the control binders that were made of raw EAF slags and cured without carbonation

TABLE 3 | Modified Tessier sequential extraction methods (Tan et al., 1997; Wei et al., 2010).

Step	Speciation	Sequential extraction condition
I	Exchangeable metals	100 ml CH_3COONa solution (1 mol/L, pH = 8.2). Shaking extraction was continued for 1 h at ambient temperature
II	Metals bound to carbonates	100 ml CH_3COONa solution (1 mol/L, pH was adjusted to 5.0 with CH_3COOH). Shaking extraction was continued for 4 h at ambient temperature
III	Metals bound to Fe/Mn oxides	Shaking extraction was continued for 5 h at 96°C with 100 ml NH_2OH·HCl-CH_3COOH solution (0.04 mol/L), volume fraction (25%)
IV	Metals bound to sulfide compounds	15 ml 0.02 mol/L HNO_3 solution and 25 ml 30%H_2O_2 (pH was adjusted to 2.0 with HNO_3 solution). Shaking extraction was continued for 3 h at 85°C, 25 ml NH_4OAc-HNO_3 solution (3.2 mol/L, 20%) was added to the cooled solution and diluted to 100 ml by deionized water. Shaking was continued for 30min
V	Residue	Digested by HNO_3+HCl + H_2O_2+HF (1:3:1:3) with a microwave

in **Table 2**, C2C represents the carbonation applied both during the pretreatment of EAF slags and after the demoulding of steel slag paste binders, A2C indicates the carbonation applied only the post-curing treatment of the demoulding paste binders, and A2A refers to the control samples that were pretreated and cured without carbonation. The hot-stage CO_2 pretreatment was applied during the pretreatment of EAF slags (SS) by importing the high purity CO_2 gas into the tube reactor (T = 650°C, 99.9 vol% CO_2 gas stream, and the atmospheric pressure), producing the carbonated EAF slags (CSS). The blend consisted of 80% SS/CSS and 20% RC was obtained by premixing the raw materials in a tumbling mixer. The water, and blend used to fabricate a paste specimen were mixed at a constant water-to-blend ratio of 0.4:1. The specimens were cast as follows: the dry-mixing of the blend were mixed for 3 minutes to ensure uniformity in the dry mix, after which water was added to the mixture, which was then mixed for a further 5 minutes. The paste binders were then cast into a 30 mm × 30 mm × 30 mm mold, prepared for the mineralogical and microstructural characterization. The pastes were demolded after curing in a standard curing chamber (T = 20 ± 2°C, RH ≥ 90%) for 24 h; and then A2A paste specimens transferred back into the curing chamber until 28 days curing age, the A2C paste and C2C paste specimens were placed immediately into a sealed carbonation chamber of 99.9 vol% CO_2 concentration, 0.1 MPa CO_2 pressure, and a temperature of 25 ± 2°C for 24 h, respectively. The pastes were broken into pieces with an iron hammer and immersed in absolute ethyl alcohol for 24 h to stop the further reaction. The pieces for mineralogical analysis, sequential leaching, and surface atomic concentration analysis were grounded into powders with an agate mortar. The pieces for microstructural analysis were dried in a vacuum oven with silica gel at 50°C for 24 h.

Testing and Characterization

XRF analyses of the reference cement and steel slags were conducted on the equipment of ARLAdvant'X Intellipower 3,600. The f-CaO contents of the steel slags were determined using the ethylene glycol method according to the China Industry Standard 4,328-2012. The f-MgO contents of the steel slags were determined using the ammonium chloride-ethylene glycol method (Ma, et al., 2017; Ma, et al., 2020). The carbonation efficiency, formation, and decomposition of $CaCO_3$ of the steel slag binders were analyzed by TG-DSC analysis (NETZSCH STA 449 F3) under N_2 atmosphere at a heating rate of 10°C/min from 35°C to 1,200°C. The minerals of the obtained samples were identified by Bruker D8 Advance XRD equipment with Cu Kα (λ = 0.15406 nm) ray from 10° to 70°. The Fourier transform infrared spectra (FTIR) were recorded on an infrared spectrometer (Nicolet IS5). The morphologies and microstructure of the binders were observed by scanning electron microscopy (SEM) coupled with energy dispersive spectroscopy (EDS) (Hitachi S-4,800). The pore size distribution were analyzed by a BET analyzer (Micromeritics ASAP2460). The Mastersizer 2,000 laser granularity meter was used to measure the particle size distribution. The surface atomic concentration and chemical states of the obtained samples were determined by a XPS spectrometer (Thermo Fisher K-alpha). The procedure of Tessier sequential extraction was that the sequential

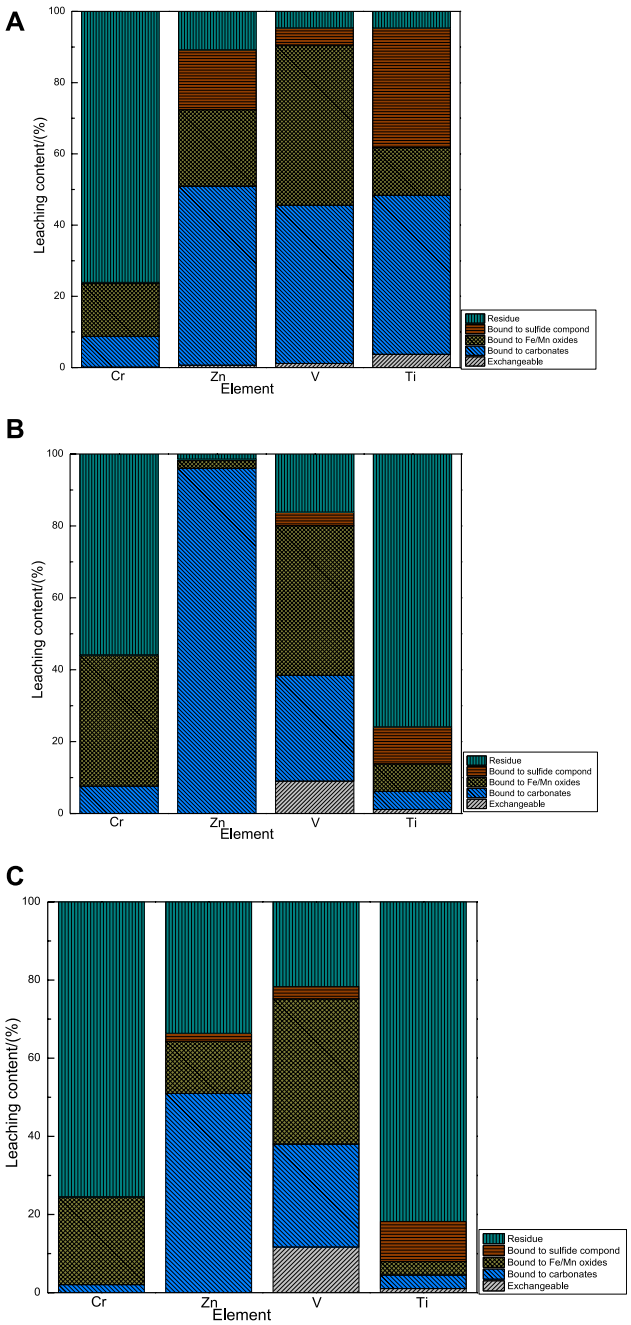

FIGURE 3 | Fraction of trace elements speciation of the uncarbonated area sample from A2A, carbonated area samples from A2C and C2C in 1d curing age. **(A)** the Cr, Zn, V, and Ti leaching content of A2A; **(B)** the Cr, Zn, V, and Ti leaching content of A2C; **(C)** the Cr, Zn, V, and Ti leaching content of C2C.

leaching characteristics of the metal combined in the paste binders were conducted according to the methods (Tan et al., 1997; Bacon and Davidson, 2008) shown in **Table 3**. The metal concentrations of the leaching solution were tested by the ICP-OES (inductively coupled plasma optical emission spectrometer, Optima 7000DV).

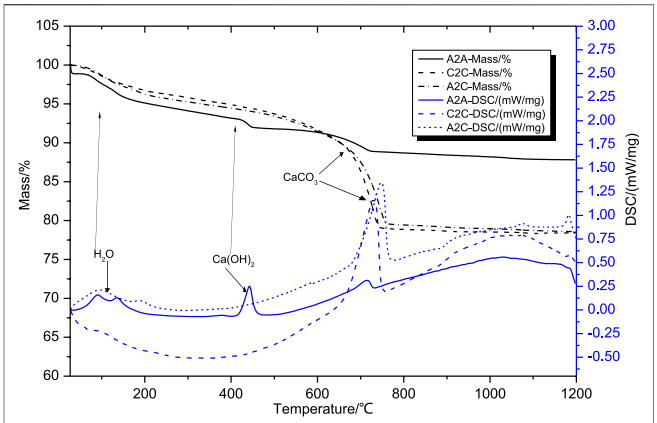

FIGURE 4 | TG-DSC analysis of the uncarbonated area sample from A2A-28d, carbonated area samples from A2C, and C2C in 1d curing age.

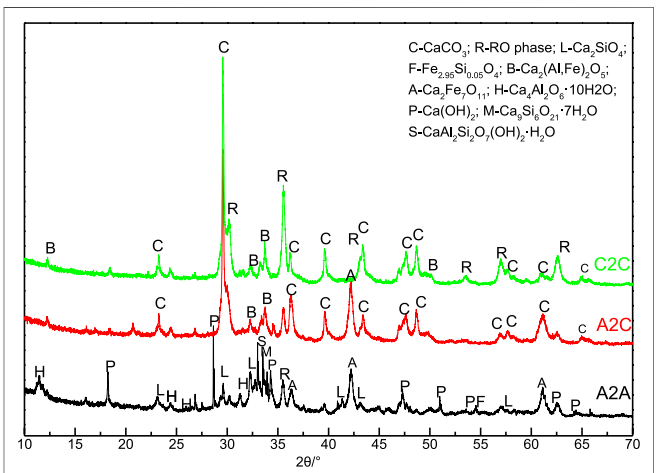

FIGURE 5 | X-ray diffraction patterns of the uncarbonated area sample from A2A-28d, carbonated area samples from A2C, and C2C in 1d curing age. (C, R, L, B, A, H, P, M, and S denote calcite ($CaCO_3$), RO phase, larnite (Ca_2SiO_4), brownmillerite ($Ca_2(Al,Fe)_2O_5$), calcium iron oxide ($Ca_2Fe_7O_{11}$), hydrocalumite($Ca_4Al_2O_6{\cdot}10H_2O$), portlandite(Ca(OH)2), metajennite ($Ca_9Si_6O_{21}{\cdot}7H_2O$), and lawsonite ($CaAl_2Si_2O_7(OH)_2{\cdot}H_2O$), respectively.)

RESULTS AND DISCUSSION

Sequential Leachability

The fraction of the trace elements (chromium, zinc, vanadium, and titanium) in the sequential leachates is presented in **Figure 3**. The accumulated active phase fraction of chromium (the sum of exchangeable chromium and chromium combined with carbonates) in the A2A, A2C, and C2C samples was 8.79, 7.62, and 2.06%, respectively. Meanwhile, the accumulated inactive phase fraction of chromium (the sum of chromium combined with Fe/Mn oxides, sulfide compounds, and the residue) in the A2A, A2C, and C2C samples were 91.21, 92.38, and 97.94%, respectively. Cr of the EAF slag paste binders gradually transformed into the inactive phases with the increase of the

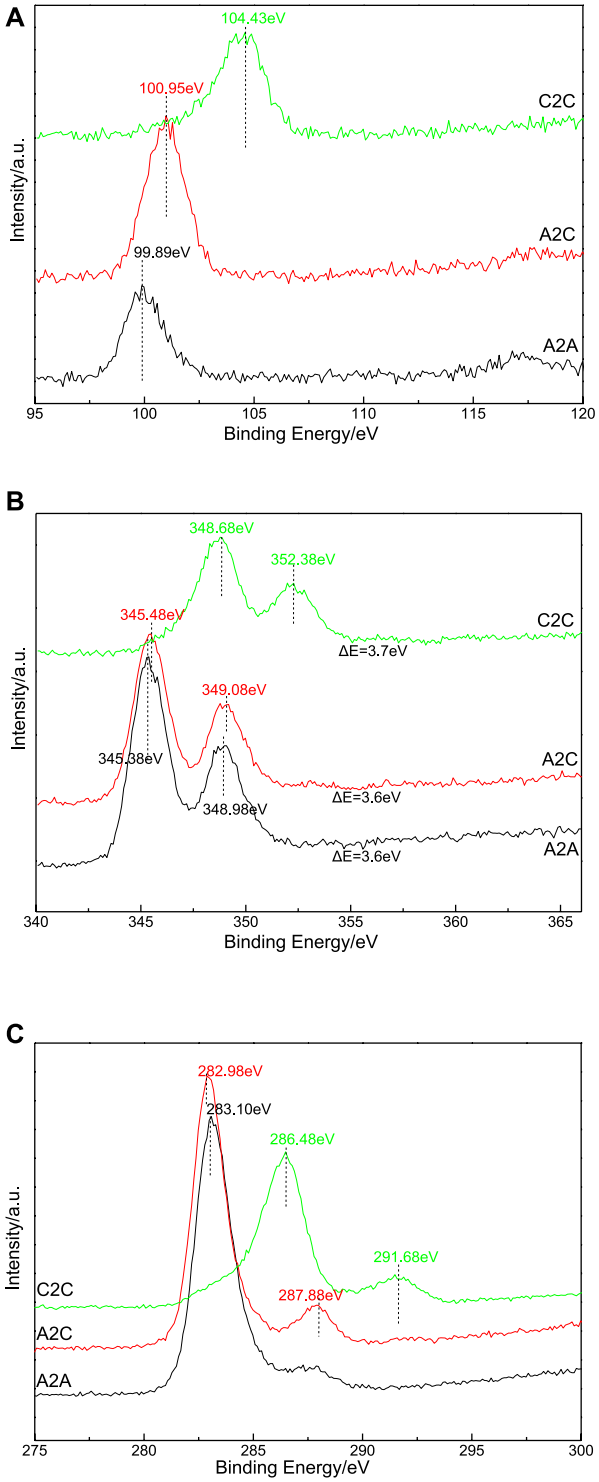

FIGURE 6 | Si 2p **(A)**, Ca 2p **(B)** and C 1s **(C)** XPS spectra of the uncarbonated area sample in A2A-28d and carbonated area samples in A2C-1d and C2C-1d.

carbonation efficiency, which was similar to the accumulated leaching results of vanadium, and titanium. In contrast, zinc of the EAF slag paste binders appeared the opposite trend.

The chromium oxides in the EAF slags existed in the form of non-hydrolyzable spinel phases or hydrolyzable silicate phases (Alejandro et al., 2011), and the zinc mineral compounds existed in zinc oxide and zinc ferrite (franklinite, $ZnFe_2O_4$) (Machado et al., 2006; Chen et al., 2011). The leaching of chromium, and zinc from in the Cr-bearing spinel phases, Mg-bearing spinel phases, and zinc ferrite phase were considered to be limited or even negligible (Zhao et al., 2019). Theoretically, the phases $MgCr_2O_4$, and $ZnFe_2O_4$ were carbonated by one static carbonation process. According to the thermodynamic data of the carbonatable mineral phases and the van't Hoff equation, ΔG^{θ} is the standard Gibbs free energy change, to determine the effect of the reaction factors and to judge the direction of the reaction. Based on the equilibrium equation of CO_2 and the mineral phases, the ΔG^{θ} of the carbonation of $MgCr_2O_4$ (−22 kJ/mol) were less than that of Ca_2SiO_4 (−116 kJ/mol), CaO (−135 kJ/mol), and MgO (−61 kJ/mol) at 298 K (Wang et al., 2020), and the ΔG^{θ} of the carbonation of $ZnFe_2O_4$ (−14 kJ/mol) were also less, which indicated that these phases were stable and carbonated just to a less extent. The carbon efficiency was increased to that of C2C, which indicated that some parts of $MgCr_2O_4$ and $ZnFe_2O_4$ were involved in the carbonation. The separated Cr_2O_3 and Fe_2O_3 were hydrolyzed as one primary phase during the leaching (Li and Tsai, 1993).

TG-DSC Analysis

The TG-DSC curves of the uncarbonated area samples from A2A, carbonated area samples from A2C, and C2C after 1 day of curing age are shown in **Figure 4**. There were weight loss steps ranging from 25°C to 200°C, from 420°C to 460°C, and from 400°C to 750°C in the A2A curve, which corresponded to the removal of bound water and physically absorbed water, the decomposition of $Ca(OH)_2$, and the decomposition of calcite (Wang et al., 2018). The A2C and C2C samples showed one remarkable weight loss step ranging from 400°C to 950°C, corresponding to the breakdown of amorphous calcite (from 400°C to 700°C) and crystallized calcite (from 700°C to 950°C) (Jeong et al., 2017). The carbonation efficiency (hereinafter referred to as EOC) was widely used to estimate the carbonation performance of various building materials or solid wastes (Chang and Fang, 2015; Liu and Wang, 2018). The EOCs of the A2A, A2C, and C2C samples were 3.3, 52, and 67%, respectively. The maximum carbonation efficiency of the binders was achieved by the simultaneous application of hot-stage CO_2 pretreatment and accelerated carbonation curing routes.

XRD Patterns

The XRD patterns of the three samples are shown in **Figure 5**. The A2A-28 days sample mainly consisted of the hydration product of the calcium silicates, such as some amorphous C-S-H gels, that cannot be detected though XRD; all of hydration products are prone to take part in the carbonation reaction and mainly produce carbonation products, such as calcite and monocarbonate (Wang et al., 2019). There were diffraction peaks of calcite were in the XRD patterns when the A2 paste was subjected to the accelerated carbonation curing treatment (Yu and Wang, 2011). The peaks of calcite were more prominent

TABLE 4 | XPS fitting analysis of valence of Cr ions at A2A-28d, A2C-1d, and C2C-1d samples.

Sample	Area(P) CPS.eV (Cr^{2+})	Area(P) CPS.eV (Cr^{3+})	Area(P) CPS.eV (Cr^{6+})	Atom% (Cr^{2+})	Atom% (Cr^{3+})	Atom% (Cr^{6+})
A2A-28d	68.25	48.39	32	45.77	32.61	21.63
A2C-1d	—	66.84	146.03	—	31.29	68.71
C2C-1d	—	52.54	34.83	—	60.05	39.96

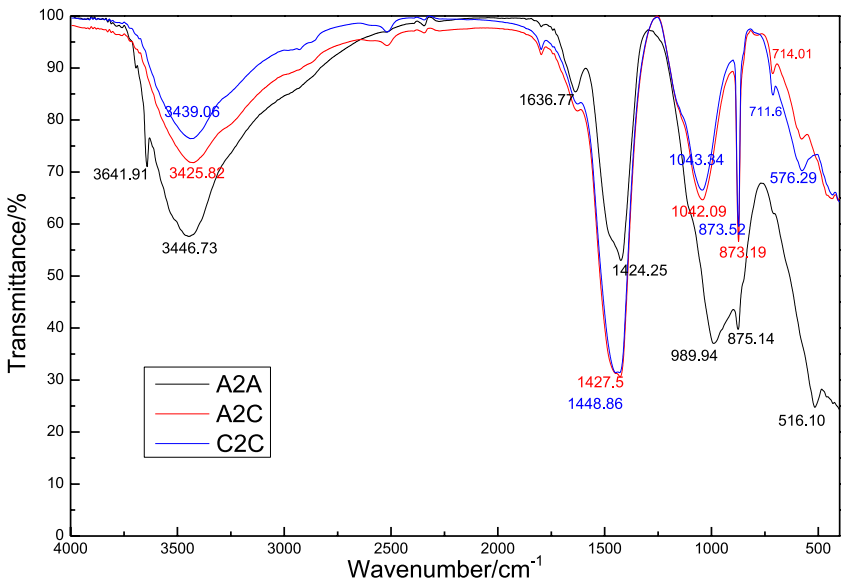

FIGURE 7 | FTIR spectra of the uncarbonated area sample from A2A-28d, carbonated area samples from A2C-1d, and C2C-1d.

when the steel slag was used instead of the A2 EAF slag mixture under hot-stage CO_2 pretreatment and the paste was put into the accelerated carbonation. These results suggested that Ca-bearing minerals were carbonated, which corresponded to the results of the phenolphthalein indicator testing and thermodynamic calculation (Wang et al., 2019). The calcite existed in the crystalline and amorphous forms, and the content of $CaCO_3$ cannot be obtained by XRD analysis, which was demonstrated by the TG-DSC study.

XPS Analysis

XPS analysis results are shown in **Figure 6** and **Table 4** to demonstrate the chemical state of the elements in the A2A-28d, A2C-1d, and C2C-1d test samples. The Si 2p peaks of the A2A-28d, A2C-1d, and C2C-1d test samples were respectively located at 99.89, 100.95, and 104.43 eV, which indicated that the binding energy of Si 2p increased after the carbonation treatments. The loss of non-bridging oxygens (Si–O–Ca moieties etc.) tended to increase the Si 2p binding energy and related silicate polymerization (Black et al., 2003b). The carbonation reaction increased the consumption of the calcium, leading to a decrease in the Ca/Si ratio, and ultimately forming a Q4 silicate (Black et al., 2007) and calcite (Richardson, 1999). The researchers (Black et al., 2003a; Black et al., 2006; Okada et al., 1998) found that the binding energy of Si had contributed to that of silicate tetrahedral polymerization. The researchers (Black et al., 2004) discovered that there was a strong negative correlation between the Si binding energy and Ca/Si ratio in the Ca-bearing and Si-bearing hydrates phase. The Si 2p peaks of the A2C and C2C samples shifted to higher binding energy, which was slightly broader than that of A2A and consistent with the EOC trend. The broadening of the peak indicated the silicate structure with a higher disorder. There were Ca 2p3/2 and Ca 2p1/2 peaks in the Ca 2p XPS spectra. The changing trend of the Ca binding energy peaks resembled that of Si, and the centre order of the Ca binding energy peak was roughly determined as C2C > A2C > A2A, which suggested that the enhancement of carbonation reaction led to the increase of the Ca binding energy. The C2C sample had much broader Ca 2p binding energy peaks than A2C and A2A, which was due to the differences in the diversity of the products (monocarbonate, calcium carbonates, or Ca and Si-bearing hydrates of the C2C sample). The C 1s peaks of the A2A-28d, A2C-1d, and C2C-1d test samples at lower binding energy were respectively located at 283.10, 282.98, and 286.48 eV, which was assigned to as “adventitious carbon” (Black et al., 2008). The C 1s peaks at higher binding energy (only at 287.88 and 291.68 eV in the A2C-1d and C2C-1d samples) were attributed to carbonate species by combining with the Ca 2p spectra. The carbonation

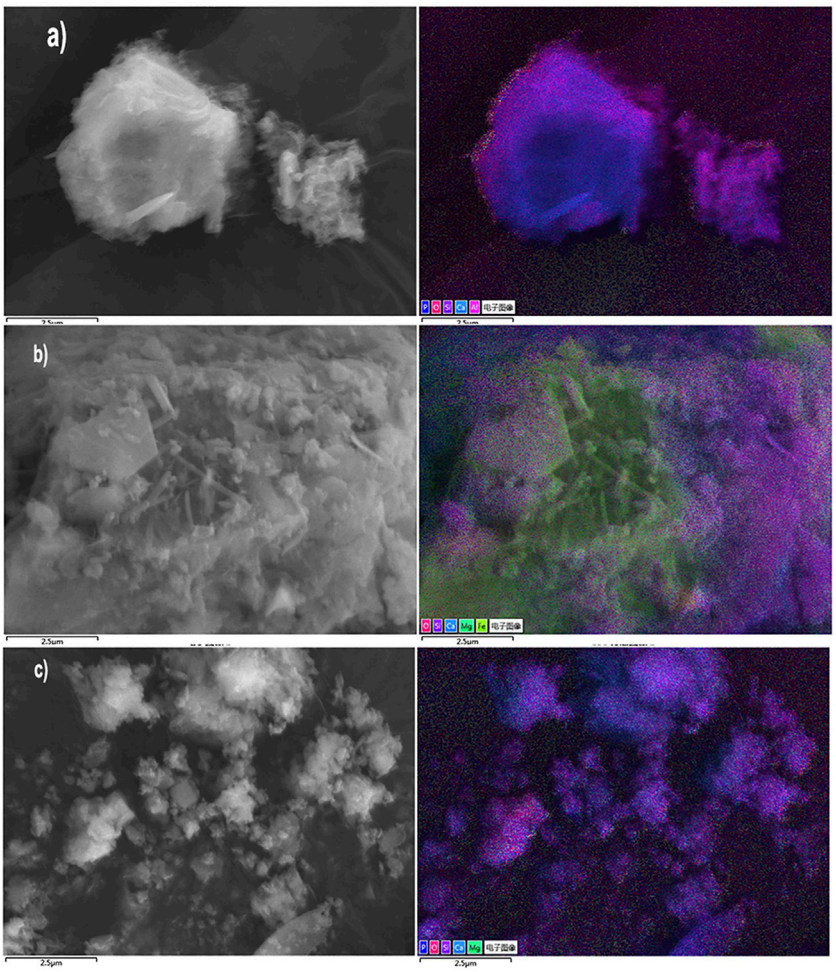

FIGURE 8 | SEM-EDS images of the uncarbonated area sample from A2A-28d **(A)**, carbonated area samples from A2C-1d **(B)**, and C2C-1d **(C)**.

of the A2C-1d and C2C-1d samples was slight, and there was one carbonate peak just about visible in the XPS spectra (Gonzalez-Elope et al., 1990). There were binding energy peaks of Cr^{2+}, Cr^{3+}, and Cr^{6+} in the Cr 2p XPS spectra, and the valence analysis results are listed in **Table 4**. According to the literature (Wang et al., 2015), the steel slag had the characteristic peak of Cr, such as Cr^{2+}, Cr^{3+}, and Cr^{6+}, and the valence states of Cr^{2+} and Cr^{3+} were the main occurrence forms. When pH ≥ 11, most of Cr^{6+} exists in the form of CrO_4^{2-}, when pH < 1.2, most of them exist in the form of $Cr_2O_7^{2-}$; under alkaline conditions, Cr^{3+} mainly exists in the form of $Cr(OH)_3$, and under acidic conditions, Cr^{3+} exists in the form of ions (Wei et al., 2010). Cr^{6+} partly transformed into Cr^{3+} due to the influence of other elements and partial pressure during the treatment (Silva and Monteiro, 2007). The changing trend of the Cr 2p binding energy peaks resembled that of Si 2p after carbonation treatment, the fraction of Cr^{3+} in the C2C sample was far greater than that of the A2A sample, which indicated that carbonate formation, mineralogical changes and the decrease of pH (lower pH) promote the leaching of one oxidation state of Cr or different leaching rates of Cr valences, corresponding to other research results (Wu et al., 2016). XPS is a general semi-quantitative analysis method for analysing the valence states of Cr element, only reflecting the surface atomic characteristics. The valence distribution of Cr can be studied by simplifying the composition of the slag and other analysis methods.

FTIR Analysis

Figure 7 shows the FT-IR spectra of the uncarbonated area in the A2A-28d sample and carbonated area in the A2C-1d and C2C-1d samples. There were asymmetric stretching (υ_3) vibration peaks of $[CO_3]^{2-}$ at 1,424.25, 1,427.5, and 1,448.86 cm^{-1} in these samples (Chang et al., 2019). The out-of-plane bending (υ_4) peaks of the C-O bond in calcite (Vagenas et al., 2003) were located at 875.14, 873.19, and 873.52 cm^{-1}. The in-plane bending peaks (υ_2) of the C-O bond in the aragonite and calcite (Chang et al., 2016) were centered at 714.01 and 711.6 cm^{-1}. The carbonation promoted the formation of crystalline and amorphous calcite. The asymmetric stretching peaks (υ_3) of

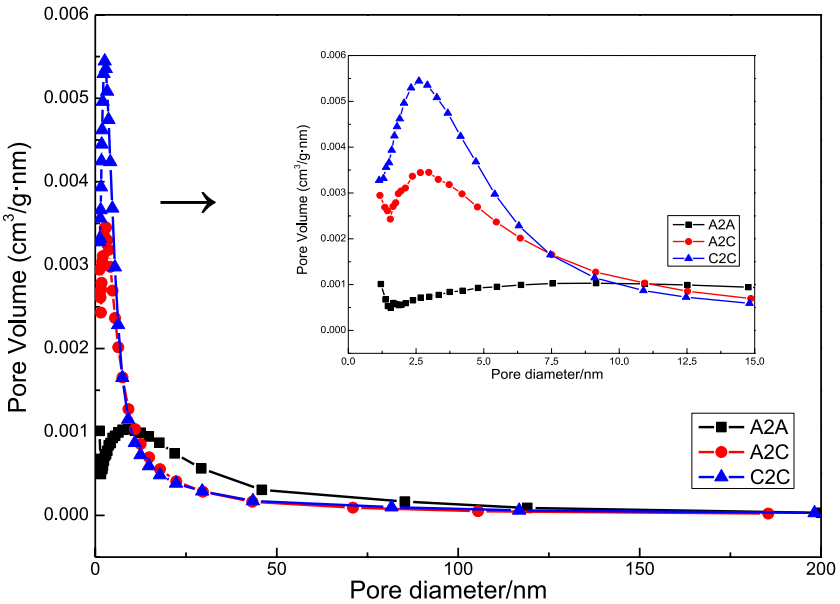

FIGURE 9 | Pore size distribution of the uncarbonated area sample in A2A-28d and carbonated area samples in A2C-1d and C2C-1d.

the Si-O bond in the silica gel (Ukwattage et al., 2015) were located at 989.94, 1,042.09, and 1,043.34 cm^{-1}, and the out-of-plane bending (υ_4) of the Si-O bond (Moon and Choi, 2019) were detected at 516.10, 568.7, and 576.29 cm^{-1}, which indicated the formation of silica gel during carbonation. The peaks at 3,640–3,645 cm^{-1} were assigned to the stretching vibration of the O-H bond, while the peaks at 3,420–3,450 cm^{-1} were contributed to the vibration of the H_2O bond in the hydration products (Lukas, 1976). Compared with the uncarbonated sample of A2A, the bands of the carbonated samples at 870–880 cm^{-1} decreased, but the bands at 510–580, 700–750, 1,000–1,100, and 1,400–1,500 cm^{-1} increased, which represented that the calcium silicates gradually reacted with CO_2 to form calcites and silica gels during the carbonation.

SEM-EDS Analysis

Figure 8 shows SEM-EDS images of these samples. According to the A2A and A2C images, the iron-containing substances (such as RO phase and brownmillerite) were involved in the carbonation reaction just to a less extent, and the uncarbonated calcium silicates core surrounded the Ca-leached and Si-rich layers (Quaghebeur et al., 2015). Physical encapsulation of the carbonate, which generated under such a carbonation ratio, reduced the hydrolysis of the primary mineral phases and then immobilized the metal, such as chromium (Spanka et al., 2016).

BET Analysis

The total pore volume, and average pore size of the original slag, carbonated slag, A2A-28d, A2C-1d, and C2C-1d steel slag-based binders are shown in **Figure 9**. By comparing the pore size distribution curves of the samples (as shown in **Figure 9**), the proportion of 2.5–10 nm mesopores of sample A2C and C2C is higher than that of sample A2A, which would result in higher performance. The average pore sizes of the three samples were 17.44, 7.22, and 6.77 nm, respectively. The pore size was reduced in the blocks, which was caused by the newly formed calcites and silica gels covering the pores of the matrix and precipitates joining together (Pizzol et al., 2014; Muller and Scrivener, 2017). The above findings fully vindicated that both carbonation processes reduced the pore area and porosity of the reaction matrix, thus promoting strength.

CONCLUSION

In conclusion, the carbonation processes of the steel slag binders were investigated, and the relationship between the carbon efficiency of the carbonation processes and the metal leachability as well as valence states minerals changes. The synergistic use of hot-stage CO_2 pretreatment and accelerated carbonation curing obtained the maximum CO_2 storage of 52% based on the binders of 80% steel slags. The hot-stage carbonation treatment facilitated particle agglomeration, minerals remodeling, and calcite formation. The carbonation curing of the steel slag paste resulted in the formation of the amorphous $CaCO_3$, calcite crystalline and Si-bearing hydrates that covered the pores of the matrix, and silicate structure with a higher disorder. The C2C binder had the lowest leachability of chromium, vanadium, and titanium, and the A2C binder had the lowest leachability of zinc. The exchangeable leachability of chromium was 1.99 mg/kg in the A2A binder, which declined to below the detection limit in the A2C sample and C2C binder after two carbonation processes. The comprehensive utilization of hot-stage carbonation and accelerated carbonation curing methods prevented the leaching of harmful metals, which provided one

reference on the reuse of steel slags as the raw building materials in one higher and more friendly way.

DATA AVAILABILITY STATEMENT

The original contributions presented in the study are included in the article/Supplementary Material, further inquiries can be directed to the corresponding author.

AUTHOR CONTRIBUTIONS

YL: Conceptualization; Methodology; Investigation; Data curation; Formal analysis; writing-original draft. JF: Funding acquisition; Writing—Review Editing. SL: Writing—Review Editing. XA: Conceptualization. YK: Investigation. LW: Investigation; Supervision.

FUNDING

This research is funded by The National Key Research and Development Program of China—Intergovernmental International Cooperation in Scientific and Technological Innovation (Grant Number 2018YFE0107300). The work described here was supported financially by MOST, the Ministry of Science and Technology of the People's Republic of China for funding this research.

REFERENCES

Cruz-Ramírez, A., Romo-Castañeda, J., Hernández-Pérez, M. d. l. Á., Vargas-Ramírez, M., Romero-Serrano, A., and Hallen-López, M. (2011). An Application of Infrared Analysis to Determine the Mineralogical Phases Formation in Fluxes for Thin Slab Casting of Steel. *J. Fluorine Chem.* 132 (5), 323–326. doi:10.1016/j.jfluchem.2011.02.019

Baciocchi, R., Costa, G., Di Gianfilippo, M., Polettini, A., Pomi, R., and Stramazzo, A. (2015). Thin-film versus Slurry-phase Carbonation of Steel Slag: CO2 Uptake and Effects on Mineralogy. *J. Hazard. Mater.* 283, 302–313. doi:10.1016/j.jhazmat.2014.09.016

Bacon, J. R., and Davidson, C. M. (2008). Is There a Future for Sequential Chemical Extraction. *Analyst* 133, 25–46. doi:10.1039/b711896a

Belhadj, E., Diliberto, C., and Lecomte, A. (2012). Characterization and Activation of Basic Oxygen Furnace Slag. *Cement and Concrete Composites* 34 (1), 34–40. doi:10.1016/j.cemconcomp.2011.08.012

Black, L., Garbev, K., Stemmermann, P., Hallam, K. R., and Allen, G. C. (2003a). Characterisation of Crystalline C-S-H Phases by X-ray Photoelectron Spectroscopy. *Cement Concrete Res.* 33, 899–911. doi:10.1016/S0008-8846(02)01089-X

Black, L., Stumm, A., Garbev, K., Stemmermann, P., Hallam, K. R., and Allen, G. C. (2003b). X-ray Photoelectron Spectroscopy of the Cement Clinker Phases Tricalcium Silicate and β-dicalcium Silicate. *Cement Concrete Res.* 33, 1561–1565. doi:10.1016/S0008-8846(03)00097-8

Black, L., Garbev, K., Stemmermann, P., Hallam, K. R., and Allen, G. C. (2004). X-ray Photoelectron Study of Oxygen Bonding in Crystalline C?S?H Phases. *Phys. Chem. Minerals* 31, 337–346. doi:10.1007/s00269-004-0401-3

Black, L., Garbev, K., Beuchle, G., Stemmermann, P., and Schild, D. (2006). X-ray Photoelectron Spectroscopic Investigation of Nanocrystalline Calcium Silicate Hydrates Synthesised by Reactive Milling. *Cement Concrete Res.* 36, 1023–1031. doi:10.1016/j.cemconres.2006.03.018

Black, L., Breen, C., Yarwood, J., Garbev, K., Stemmermann, P., and Gasharova, B. (2007). Structural Features of C?S?H(I) and its Carbonation in Air?A Raman Spectroscopic Study. Part II: Carbonated Phases. *J. Am. Ceram. Soc.* 90, 908–917. doi:10.1111/j.1551-2916.2006.01429.x

Black, L., Garbev, K., and Gee, I. (2008). Surface Carbonation of Synthetic C-S-H Samples: A Comparison between Fresh and Aged C-S-H Using X-ray Photoelectron Spectroscopy. *Cement Concrete Res.* 38, 745–750. doi:10.1016/j.cemconres.2008.02.003

Carvalho, S. Z., Vernilli, F., Almeida, B., Demarco, M., and Silva, S. N. (2017). The Recycling Effect of BOF Slag in the Portland Cement Properties. *Resour. Conservation Recycling* 127, 216–220. doi:10.1016/j.resconrec.2017.08.021

Chang, J., and Fang, Y. (2015). Quantitative Analysis of Accelerated Carbonation Products of the Synthetic Calcium Silicate hydrate(C-S-H) by QXRD and TG/MS. *J. Therm. Anal. Calorim.* 119, 57–62. doi:10.1007/s10973-014-4093-8

Chang, J., Fang, Y., and Shang, X. (2016). The Role of β-C2S and γ-C2S in Carbon Capture and Strength Development. *Mater. Struct.* 49, 4417–4424. doi:10.1617/s11527-016-0797-5

Chang, J., Xiong, C., Zhang, Y., and Wang, D. (2019). Foaming Characteristics and Microstructure of Aerated Steel Slag Block Prepared by Accelerated Carbonation. *Construction Building Mater.* 209, 222–233. doi:10.1016/j.conbuildmat.2019.03.077

Chen, W.-S., Shen, Y.-H., Tsai, M.-S., and Chang, F.-C. (2011). Removal of Chloride from Electric Arc Furnace Dust. *J. Hazard. Mater.* 190, 639–644. doi:10.1016/j.jhazmat.2011.03.096

Dong, X. D. (2008). Preliminary Experiments on Fast Absorption of CO_2 by Steel Slag of Converter. *Steelmaking* 24 (5), 29–32. CNKI:SUN:LGZZ.0.2008-05-013.

Eloneva, S., Puheloinen, E.-M., Kanerva, J., Ekroos, A., Zevenhoven, R., and Fogelholm, C.-J. (2010). Co-utilisation of CO2 and Steelmaking Slags for Production of Pure CaCO3 - Legislative Issues. *J. Clean. Prod.* 18, 1833–1839. doi:10.1016/j.jclepro.2010.07.026

Gonzalez-Elope, A. R., Espinos, J. P., Femandez, A., and Munuera, G. (1990). XPS Study of the Surface Carbonation/Hydroxylation State of Metal Oxides. *Appl. Surf. Sci.* 45, 103–108. doi:10.1016/0169-4332(90)90060-D

Guo, J., Bao, Y., and Wang, M. (2018). Steel Slag in China: Treatment, Recycling, and Management. *Waste Management* 78, 318–330. doi:10.1016/j.wasman.2018.04.045

Jeong, Y., Yum, W. S., Moon, J., and Oh, J. E. (2017). Utilization of Precipitated CaCO3 from Carbon Sequestration of Industrially Emitted CO2 in Cementless CaO-Activated Blast-Furnace Slag Binder System. *J. Clean. Prod.* 166, 649–659. doi:10.1016/j.jclepro.2017.08.097

Kim, E., Spooren, J., Broos, K., Nielsen, P., Horckmans, L., Geurts, R., et al. (2016). Valorization of Stainless Steel Slag by Selective Chromium Recovery and Subsequent Carbonation of the Matrix Material. *J. Clean. Prod.* 117, 221–228. doi:10.1016/j.jclepro.2016.01.032

Li, C. L., and Tsai, M. S. (1993). A crystal Phase Study of Zinc Hydroxide Chloride in Electric-Arc-Furnace Dust. *J. Mater. Sci.* 28, 4562–4570. doi:10.1007/BF00414243

Liu, Y. J., and Wang, L. (2018). Carbonation Mechanism of New Low-Calcium Air-Setting Portland Cement. *New Build. Mater.* 45 (01), 109–113. doi:10.3969/j.issn.1001-702X.2018.01.028

Lukas, W. (1976). Substitution of Si in the Lattice of Ettringite. *Cement Concrete Res.* 6, 225–233. doi:10.1016/0008-8846(76)90120-4

Ma, L. J., Lian, F., Wang, H. X., and Zhang, Z. S. (2017). Determination and Reduction of Free Periclase in Steel Slag. *Multipurp. Utiliz. Miner. Resour.* 5, 70–75. doi:10.3969/j.issn.1000-6532.2017.05.015

Ma, Z., Yao, Y., Liu, Z., Wei, L., Wu, B., Wen, Z., et al. (2020). A New Technique to Quantitatively Determine the Periclase Content in High Magnesia Portland Cement. *Front. Mater.* 7. doi:10.3389/fmats.2020.00225

Machado, J., Brehm, F., Moraes, C., Santos, C., Vilela, A., and Cunha, J. (2006). Chemical, Physical, Structural and Morphological Characterization of the Electric Arc Furnace Dust. *J. Hazard. Mater.* 136, 953–960. doi:10.1016/j.jhazmat.2006.01.044

Miranda-Pizarro, J., Perejón, A., Valverde, J. M., Sánchez-Jiménez, P. E., and Pérez-Maqueda, L. A. (2016). Use of Steel Slag for CO2 Capture under Realistic

Calcium-Looping Conditions. *RSC Adv.* 6 (44), 37656–37663. doi:10.1039/C6RA03210A

Mo, L., Zhang, F., Deng, M., Jin, F., Al-Tabbaa, A., and Wang, A. (2017). Accelerated Carbonation and Performance of concrete Made with Steel Slag as Binding Materials and Aggregates. *Cement and Concrete Composites* 83, 138–145. doi:10.1016/j.cemconcomp.2017.07.018

Moon, E.-J., and Choi, Y. C. (2019). Carbon Dioxide Fixation via Accelerated Carbonation of Cement-Based Materials: Potential for Construction Materials Applications. *Construction Building Mater.* 199, 676–687. doi:10.1016/j.conbuildmat.2018.12.078

Muller, A. C. A., and Scrivener, K. L. (2017). A Reassessment of Mercury Intrusion Porosimetry by Comparison with 1H NMR Relaxometry. *Cement Concrete Res.* 100, 350–360. doi:10.1016/j.cemconres.2017.05.024

Okada, K., Kameshima, Y., and Yasumori, A. (1998). Chemical Shifts of Silicon X-ray Photoelectron Spectra by Polymerization Structures of Silicates. *J. Am. Ceram. Soc.* 81, 1970–1972. doi:10.1111/j.1151-2916.1998.tb02579.x

Pan, S.-Y., Adhikari, R., Chen, Y.-H., Li, P., and Chiang, P.-C. (2016). Integrated and Innovative Steel Slag Utilization for Iron Reclamation, green Material Production and CO2 Fixation via Accelerated Carbonation. *J. Clean. Prod.* 137, 617–631. doi:10.1016/j.jclepro.2016.07.112

Pan, S.-Y., Chung, T.-C., Ho, C.-C., Hou, C.-J., Chen, Y.-H., and Chiang, P.-C. (2017). CO2 Mineralization and Utilization Using Steel Slag for Establishing a Waste-To-Resource Supply Chain. *Sci. Rep.* 7, 17227. doi:10.1038/s41598-017-17648-9

Pasetto, M., and Baldo, N. (2016). Recycling of Waste Aggregate in Cement Bound Mixtures for Road Pavement Bases and Sub-bases. *Construction Building Mater.* 108, 112–118. doi:10.1016/j.conbuildmat.2016.01.023

Pizzol, V. D., Mendes, L. M., Frezzatti, L., Savastano Jr., H., Jr., and Tonoli, G. H. D. (2014). Effect of Accelerated Carbonation on the Microstructure and Physical Properties of Hybrid Fiber-Cement Composites. *Minerals Eng.* 59, 101–106. doi:10.1016/j.mineng.2013.11.007

Poh, H. Y., Ghataora, G. S., and Ghazireh, N. (2006). Soil Stabilization Using Basic Oxygen Steel Slag Fines. *J. Mater. Civ. Eng.* 18, 229–240. doi:10.1061/(ASCE)0899-1561

Polettini, A., and Pomi, R. (2004). The Leaching Behavior of Incinerator Bottom Ash as Affected by Accelerated Ageing. *J. Hazard. Mater.* 113, 209–215. doi:10.1016/j.jhazmat.2004.06.009

Quaghebeur, M., Nielsen, P., Horckmans, L., and Van Mechelen, D. (2015). Accelerated Carbonation of Steel Slag Compacts: Development of High-Strength Construction Materials. *Front. Energ. Res.* 3, 1–12. doi:10.3389/fenrg.2015.00052

Richardson, I. G. (1999). The Nature of C-S-H in Hardened Cements. *Cement Concrete Res.* 29, 1131–1147. doi:10.1016/S0008-8846(99)00168-4

Shi, C. (2004). Steel Slag-Its Production, Processing, Characteristics, and Cementitious Properties. *J. Mater. Civ. Eng.* 16 (3), 230–236. doi:10.1002/chin.200522249

Silva, D. A., and Monteiro, P. J. M. (2007). Early Formation of Ettringite in Tricalcium Aluminate?Calcium Hydroxide?Gypsum Dispersions. *J. Am. Ceram. Soc.* 90 (2), 614–617. doi:10.1111/j.1551-2916.2006.01384.x

Skaf, M., Manso, J. M., Aragón, Á., Fuente-Alonso, J. A., and Ortega-López, V. (2017). EAF Slag in Asphalt Mixes: a Brief Review of its Possible Re-use. *Resour. Conservation Recycling* 120, 176–185. doi:10.1016/j.resconrec.2016.12.009

Spanka, M., Mansfeldt, T., and Bialucha, R. (2016). Influence of Natural and Accelerated Carbonation of Steel Slags on Their Leaching Behavior. *Steel Research Int.* 87 (6), 798–810. doi:10.1002/srin.201500370

Stolaroff, J. K., Lowry, G. V., and Keith, D. W. (2005). Using CaO- and MgO-Rich Industrial Waste Streams for Carbon Sequestration. *Energ. Convers. Management* 46, 687–699. doi:10.1016/j.enconman.2004.05.009

Tan, L. C., Choa, V., and Tay, J. H. (1997). Influence of pH on Mobility of Heavy Metals from Municipal Solid Waste Incinerator Fly Ash. *Environ. Monit. Assess.* 44 (1-3), 275–284. doi:10.1023/a:1005744811206

Tian, S.-c., Jiang, J.-g., Li, K.-m., Yan, F., and Chen, X.-j. (2014). Performance of Steel Slag in Carbonation-Calcination Looping for CO2capture from Industrial Flue Gas. *RSC Adv.* 4, 6858–6862. doi:10.1039/C3RA47426G

Ukwattage, N. L., Ranjith, P. G., Yellishetty, M., Bui, H. H., and Xu, T. (2015). A Laboratory-Scale Study of the Aqueous mineral Carbonation of Coal Fly Ash for CO2 Sequestration. *J. Clean. Prod.* 103, 665–674. doi:10.1016/j.jclepro.2014.03.005

Ukwattage, N. L., Ranjith, P. G., and Li, X. (2017). Steel-making Slag for mineral Sequestration of Carbon Dioxide by Accelerated Carbonation. *Measurement* 97, 15–22. doi:10.1016/j.measurement.2016.10.057

Vagenas, N., Gatsouli, A., and Kontoyannis, C. G. (2003). Quantitative Analysis of Synthetic Calcium Carbonate Polymorphs Using FT-IR Spectroscopy. *Talanta* 59 (4), 831–836. doi:10.1016/S0039-9140(02)00638-0

Wang, G., Wang, Y., and Gao, Z. (2010). Use of Steel Slag as a Granular Material: Volume Expansion Prediction and Usability Criteria. *J. Hazard. Mater.* 184, 555–560. doi:10.1016/j.jhazmat.2010.08.071

Wang, H., Yan, B., and Li, F. (2015). Analysis of Cr with Various Valence States in Industrial EAF Slag for Making Stainless Steel. *ISIJ Int.* 55 (7), 1425–1431. doi:10.2355/isijinternational.55.1425

Wang, L., Chen, L., Tsang, D. C. W., Li, J.-S., Yeung, T. L. Y., Ding, S., et al. (2018). Green Remediation of Contaminated Sediment by Stabilization/solidification with Industrial By-Products and CO2 Utilization. *Sci. Total Environ.* 631-632, 1321–1327. doi:10.1016/j.scitotenv.2018.03.103

Wang, X., Ni, W., Li, J., Zhang, S., Hitch, M., and Pascual, R. (2019). Carbonation of Steel Slag and gypsum for Building Materials and Associated Reaction Mechanisms. *Cement Concrete Res.* 125, 105893. doi:10.1016/j.cemconres.2019.105893

Wang, Y.-J., Zeng, Y.-N., Li, J.-G., Zhang, Y.-Z., Zhang, Y.-J., and Zhao, Q.-Z. (2020). Carbonation of Argon Oxygen Decarburization Stainless Steel Slag and its Effect on Chromium Leachability. *J. Clean. Prod.* 256, 120377: 1–10. doi:10.1016/j.jclepro.2020.120377

Wei, J. X., Bai, R. Y., Yu, Q. J., and Yao, J. Y. (2010). Speciation and Distribution of Cr in Hardened Cement Paste-Modified Tessier Sequential Extraction Procedure. *J. Chin. Ceram. Soc.* 38 (7), 1167–1172. CNKI:SUN:GXYB.0.2010-07-005.

Wu, Q. F., Bao, Y. P., Lin, L., Xu, G. P., Cheng, H. G., and Xin, C. P. (2015). Study on Phase Compositions and Microstructure of Slag in Different Processes. Indus. *Saf. Environ. Protec.* 41 (08), 86–89. CNKI:SUN:GYAF.0.2015-08-024.

Wu, X., Yu, B., Xu, W., Fan, Z., Wu, Z., and Zhang, H. (2016). Stabilization of Carbon Dioxide and Chromium Slag via Carbonation. *Environ. Technology* 38, 1997–2002. doi:10.1080/09593330.2016.1244566

Yi, H., Xu, G., Cheng, H., Wang, J., Wan, Y. F., Wan, Y., et al. (2012). An Overview of Utilization of Steel Slag. *Proced. Environ. Sci.* 16, 791–801. doi:10.1016/j.proenv.2012.10.108

Yu, J., and Wang, K. (2011). Study on Characteristics of Steel Slag for CO2 Capture. *Energy Fuels* 25, 5483–5492. doi:10.1021/ef2004255

Zhao, Q., Liu, C., Cao, L., Jiang, M., Li, B., Saxén, H., et al. (2019). Shear-force Based Stainless Steel Slag Modification for Chromium Immobilization. *ISIJ Int.* 59 (3), 583–589. doi:10.2355/isijinternational.isijint-2017-678

Conflict of Interest: The authors declare that the research was conducted in the absence of any commercial or financial relationships that could be construed as a potential conflict of interest.

Publisher's Note: All claims expressed in this article are solely those of the authors and do not necessarily represent those of their affiliated organizations, or those of the publisher, the editors and the reviewers. Any product that may be evaluated in this article, or claim that may be made by its manufacturer, is not guaranteed or endorsed by the publisher.